Nonlinear Baroclinic Adjustment

PRISCILLA CEHELSKY*

Program in Applied Mathematics, University of Colorado, Boulder, Colorado

KA KIT TUNG

Department of Applied Mathematics, University of Washington, Seattle, Washington

(Manuscript received 29 May 1990, in final form 27 February 1991)

ABSTRACT

The concept of baroclinic adjustment is reexamined in the context of a fully nonlinear two-layer model on a β-plane. Based on our results we propose a single, conceptually very simple mechanism of the nonlinear equilibration of waves and the mean flow, which we term "nonlinear baroclinic adjustment." The new concept appears applicable to cases that currently require different explanations, varying from case to case, to account for the equilibration of the mean temperature gradient in the presence of external driving.

1. Introduction

The north–south temperature gradient in the mid- and high-latitude atmosphere is known to be approximately constant in the course of a year, despite large differences in solar insolation (Stone 1978). Seasonal differences in solar heating instead lead to differences of eddy heat flux (Stone 1978; Stone and Miller 1980). These properties of the atmospheric flow suggest that the effects of eddies can indeed be parameterized in climate models. To be sure, the problem of eddy flux parameterization has received considerable attention (e.g., Green 1970; Stone 1972, 1978; Moura and Stone 1976; Lindzen and Farrel 1980) because of the possibility of devising simple climate models.

Stone (1978) proposed the mechanism of baroclinic adjustment to address the overall effect of the eddies on the meridional temperature gradient. Relating the observed mean shear to the critical shear for baroclinic instability in a two-layer model, Stone postulated that the role of the eddies is to keep the temperature gradient from becoming appreciably supercritical (in the sense of a two-layer model).[1]

The above mechanism for the equilibration of the meridional temperature gradient has been deemed inappropriate in nonlinear settings (Salmon 1980; Vallis 1988). Baroclinic adjustment, as originally proposed, is governed by quasi-linear dynamics. Through interactions with the mean flow, the linearly, baroclinically most unstable wave is responsible for keeping the mean state near critical. However, two main results from nonlinear dynamics seem to preclude the applicability of this mechanism to the observed (nonlinear) atmosphere. One is the fact that waves longer than the baroclinically most unstable scales contain most of the energy and are responsible for most of the heat flux. (Observational evidence: e.g., Chen and Wiin-Nielsen 1978; Boer and Shepherd 1983; Shepherd 1987. Theoretical and numerical evidence: e.g., Simmons and Hoskins 1978; Gall et al. 1979; Hart 1981; Pedlosky 1981; Vallis and Roads 1984; Haidvogel and Held 1980; Salmon 1980; Vallis 1983; Klein and Pedlosky 1986.) And second, in nonlinear two-layer models, under very strong forcing, the equilibrated zonal shear is highly supercritical (e.g., Salmon 1980; Vallis and Roads 1974; Cehelsky and Tung 1987; Vallis 1988).

The above discrepancies led Salmon (1980) to propose several mechanisms of equilibration (see also Vallis 1988): wave–mean flow equilibration, wave–wave equilibration, and stochastic equilibration. Baroclinic adjustment comes under wave–mean flow equilibration. Wave–wave equilibration describes the nonlinear process whereby energy is transferred from the most unstable wavenumbers to stable or less unstable wavenumbers via triad interactions. Stochastic equilibration results when the correlation between perturbation meridional velocity and temperature is reduced, which, in effect, alleviates the baroclinic instability mechanism. It was speculated that different equilibration mechanisms may be effective in different parameter regimes.

While the quasi-linear baroclinic adjustment mechanism is unable to account for observed behaviors in the atmosphere and in numerical models, it is also true

[1] The relevance of the critical shear (or temperature gradient) in a two-layer model to a continuous model can be deduced from Green (1960). The critical shear of a two-layer model represents a transition, in a continuous model, from a regime in which the dominant waves are short and shallow, to one in which the dominant waves are long and deep. Furthermore, Held (1978) found that long, deep waves are the more efficient heat transporters. Instability in a two-layer model is thus representative of a regime in a continuous model, governed by long, deep, more efficient waves.

* Present affiliation: NRC Associate, NASA/GSFC, Laboratory for Atmospheres, Greenbelt, Maryland 20771.

Corresponding author address: Dr. Ka Kit Tung, Dept. of Applied Mathematics, FS-20, University of Washington, Seattle, WA 98195.

that turbulence theories (such as wave–wave and stochastic equilibration) are problematic (Shepherd 1987; Reinhold 1988). The assumptions of isotropy and horizontal homogeneity severely limit the applicability of current turbulence theories to the atmosphere. Shepherd (1987) demonstrated that while results from turbulence such as energy cascading to lower wavenumbers and the barotropization of the flow appear to be reconcilable with the observed transient eddy statistics, interactions associated with the stationary component of the atmosphere are unaccounted for.

Using a two-layer β-plane model, we will demonstrate that the equilibration of the meridional temperature gradient can be understood via a *nonlinear* baroclinic adjustment mechanism. Although there appear to be discrepancies between quasi-linear theory and results from nonlinear numerical models, in the end we find a single modified baroclinic adjustment mechanism to be responsible for all processes. Our approach is to study equilibration for a wide range of thermal forcing. Previous studies that reported supercritical equilibrated temperature gradients (e.g., Salmon 1980; Vallis 1988) considered only one value of driving for a given set of parameters, and therefore could not see the full picture. Under our proposed mechanism (which integrates several previously proposed mechanisms) the equilibrated meridional temperature gradient is maintained by the heat flux due mainly to the "most efficient" wave, the scale of which shifts up as radiative forcing is increased. At high values of radiative driving, it is the largest-scale wave permitted by the geometry that is responsible for most of the heat transport. The level of equilibration can be related to the critical gradient for linear baroclinic instability of the main heat-transporting eddies, and at high driving this level asymptotes to the critical mean temperature gradient of the largest-scale wave. It is therefore *critical* for that wave, although it is "supercritical" for the linearly most unstable wave. The latter is saturated and cannot participate in the baroclinic adjustment process. An equilibrated atmosphere, according to our conceptual model, is still unstable to the cyclone-scale waves that continue to evolve throughout their life cycles. This is in contrast to the results of classical (quasi-linear) baroclinic adjustment, which renders all scales stable, thereby excluding the baroclinic development of cyclones. Furthermore, our results remain unchanged when, in addition to self-excited baroclinic waves, topographically forced waves are present.

How generally applicable is the proposed theory? We note that some previously published results at first do not appear to fit into the scenario outlined above (Vallis 1988; Panetta and Held 1988; Cai 1991, personal communication). Specifically, these show that under certain conditions, the equilibrated temperature gradient is supercritical to all waves. However, it can be shown that, as in the case of Vallis (1988), Panetta and Held (1988), and Cai (1991, personal communication), this behavior occurs as a result of their truncating the zonal wavenumbers in their models to one (while retaining many meridional modes). This truncation artificially suppresses nonlinear wave–wave interactions. Another exception occurs in our fully nonlinear calculations when the parameter regime is such that only one zonal wavenumber is unstable. These exceptional cases will be discussed in section 5. The inferred general mechanism is summarized in section 6.

Finally, it is noted that we have not investigated the process of baroclinic adjustment via modification to the static stability. The static stability parameter in our model is held constant in all our experiments.

2. The two-layer model

The model used in this study is a two-layer channel model with β-plane geometry, originally formulated by Lorenz (1960, 1963). The quasi-geostrophic vorticity and thermodynamic equations are, in standard notation:

$$\frac{\partial}{\partial t}\nabla^2\Psi = -J(\Psi, \nabla^2\Psi) - J(\tau, \nabla^2\tau) - \beta_0\frac{\partial\Psi}{\partial x} - \frac{1}{2}\nu_E\nabla^2(\Psi - \tau) \quad (2.1)$$

$$\frac{\partial}{\partial t}\nabla^2\tau = -J(\Psi, \nabla^2\tau) - J(\tau, \nabla^2\Psi) - \beta_0\frac{\partial\tau}{\partial x} - \frac{f_0 w}{H} + \frac{1}{2}\nu_E\nabla^2(\Psi - \tau) \quad (2.2)$$

$$2\frac{\partial}{\partial t}\tau = -J(\Psi, 2\tau) - \frac{N^2 H}{f_0}w + 2h'_d(\tau^* - \tau) \quad (2.3)$$

$$\nabla^2\Theta = A\nabla^2\tau, \quad (2.4)$$

which have been finite differenced in the vertical direction. Here ψ_1 and ψ_2 are the upper- and lower-layer streamfunctions; $\Psi = (\psi_1 + \psi_2)/2$ and $\tau = (\psi_1 - \psi_2)/2$ are the mean and shear streamfunctions; Θ is the potential temperature; Θ^* is the radiative forcing; w is the vertical velocity between the layers; ν_E is the Ekman damping coefficient at the bottom surface; h'_d is the Newtonian cooling coefficient; H is the scale height; N is the Brunt–Väisälä frequency; and f_0 and β_0 are the Coriolis and beta parameters at the midchannel latitude ϕ_0.

The variables are nondimensionalized as follows: y by L, x by $L/n (n = 2L_y/L_x$, where L_y is the channel width and L_x is the channel length), t by f_0^{-1}, Ψ and τ by $L^2 f_0$, Θ by $AL^2 f_0$ (see footnote 2), w by Hf_0, and β_0 by $f_0 L^{-1}$. We now define the dimensionless constants $\beta \equiv La^{-1}\cot\varphi_0$, $\sigma_0 \equiv N^2H^2(2L^2f_0^2)^{-1}$, $2\nu \equiv \nu_E f_0^{-1}$, and $2h'' \equiv h'_d f_0^{-1}$. All variables are now nondimensional unless otherwise stated.

The parameter n is a horizontal aspect ratio: $n = 2L_y/L_x$. By varying n, the meridional channel width

can be altered relative to the zonal channel length. Alternatively, if the meridional width is fixed, then n defines the fundamental zonal harmonic. Thus, for example, for a 45° channel with $n = 0.75$, the fundamental harmonic in the model is equivalent to global zonal wavenumber 3 (i.e., $L_x = 2L_y/0.75 = 120°$), whereas with $n = 1.25$, the fundamental harmonic is equivalent to global zonal wavenumber 5. In this two-layer model, a given wave will be linearly baroclinically unstable if its wavenumber lies within the long and short wavenumber cutoffs determined by a linear stability analysis. Thus, varying n will change the number of unstable waves in the model.

The dependent variables are expanded in the orthonormal eigenfunctions, F_i, of the Laplace operator. These eigenfunctions satisfy the conditions of no flow through the lateral boundaries and no momentum convergence at the lateral boundaries. The appropriate eigenfunctions are:

$$f_{A(j)} = \sqrt{2}\cos(jy)$$
$$f_{K(k,j)} = 2\cos(knx)\sin(jy)$$
$$f_{L(k,j)} = 2\sin(knx)\sin(jy), \qquad (2.5)$$

where $j = 1, 2, \cdots, Y_T$, and $k = 1, 2, \cdots, X_T$ and Y_T and X_T are the y and x wavenumbers, respectively, beyond which the expansion is truncated. The dimension of the resulting system of ordinary differential equations is $2Y_T(2X_T + 1)$. Hereafter we will refer to a model truncated at X_T, Y_T as a (X_Tx, Y_Ty) model. The resolution we have chosen to work with is $X_T = 10$, $Y_T = 10$. This resolution is sufficient for obtaining qualitatively converged results (see Cehelsky and Tung 1987).

The notation is as follows. The coefficients in the expansions are subscripted in the same way as the respective eigenfunctions. Thus, for example, the coefficients in the mean streamfunction expansion take the forms $\psi_{A(j)}$, $\psi_{K(k,j)}$, and $\psi_{L(k,j)}$. When $k = j = 1$, the indices are omitted: $\psi_{A(1)} = \psi_A$, $\psi_{K(1,1)} = \psi_K$, and $\psi_{L(1,1)} = \psi_L$.

The thermal forcing is represented by a single zonal component

$$\Theta^*(x, y) = \theta^*_{A(1)}\sqrt{2}\cos(y) = \theta^*_A\sqrt{2}\cos(y).$$

The scaling constants in this set are $\varphi_0 = 50°$N, $L = 1600$ km (a channel width of $\pi L = 5027$ km), $a_0 = 6400$ km, $H = 7.5$ km, $f_0 = 1 \times 10^{-4}$ s^{-1}, and $A = 1.1886 \times 10^{-10}$ s K/cm^{-2}. The model parameters take on the values $\beta = 0.2$, $\sigma_0 = 0.1$, $\nu = 0.0086348$ (6 day Ekman damping time), and $h'' = 0.01036175$ (10 day Newtonian cooling time). A subgrid ∇^4 type damping [with frictional coefficient $\nu_s = 0.0003453916$ (325 days)] is used in both layers to enhance convergence. For more details about this model see Cehelsky and Tung (1987).

3. Equilibration in a simple quasi-linear case

Before discussing results from the fully nonlinear model, we will illustrate the classic baroclinic adjustment process using a quasi-linear model that permits only wave–mean flow interactions, and in which only one meridional mode is retained (the gravest mode). There is a similarity between this quasi-linear case and the nonlinear one that follows. The case without severe meridional truncation [viz., the $(1x, 10y)$ model] does not share such a similarity with the nonlinear case. It will be discussed in section 5. Without loss of generality, we will investigate the case $n = 1.3$, for which there are two baroclinically unstable zonal scales. More precisely, these are the scales $L/1n = L/1.3$ and $L/2n = L/2.6$.

Associated with two-layer models is a critical shear of the zonal wind, beyond which the basic state is baroclinically unstable. In the present class of thermally driven two-layer models, the basic state, known as the "Hadley solution," is the radiative equilibrium solution. For thermal forcing, θ^*_A, less than some critical value, the Hadley solution is stable and is the only solution the model supports. This purely zonal steady flow is found by setting all wave variables to zero and solving for the two zonal variables ψ_A and θ_A, viz.,

$$\theta_A = \frac{h''(\nu + \nu_s)\theta^*_A}{h''(\nu + \nu_s) + \sigma_0(2\nu\nu_s + \nu_s^2)} \qquad (3.1)$$

$$\psi_A = \frac{\nu\theta_A}{\nu + \nu_s}. \qquad (3.2)$$

(Note that due to the formulation of this two-layer model, θ_A is proportional to the zonal wind shear and the zonal temperature, as well as the meridional temperature gradient.)

It is instructive to consider the equation for the difference of the mean zonal temperature across the channel since this difference is a measure of the meridional temperature gradient. Taking the difference of the zonally averaged energy equation across the channel yields

$$\frac{\partial}{\partial t}\Delta\Theta = \Pi_1 + \Pi_2 - \sigma_0\Delta w + h''(\Delta\Theta^* - \Delta\Theta), \qquad (3.3)$$

where ΔS represents the difference of a quantity S across the channel, and Π_1 and Π_2 are the heat flux differences[3] across the channel due to zonal wavenumbers 1 and 2, respectively. Under radiative equilibrium, there is a balance between the last two terms of Eq. (3.3).

If perturbations are introduced into the equations, for $\Delta\Theta^*$ greater than a critical value, $\Delta\Theta^*_{\text{critical}}$, a steady-state wave solution is reached. The temperature dif-

[2] $A = 2f_0/c_p[(P_2/P_{00})^K - (P_1/P_{00})^K]$, where c_p is the specific heat at constant pressure and $K = R/c_p$ with R the universal gas constant.

[3] More precisely, Π_i is the difference across the channel of the heat flux convergence.

ference equilibrates at its critical value, $\Delta\Theta_{\text{critical}}$ (corresponding to the Hadley solution at $\Delta\Theta^*_{\text{critical}}$). Here Δw also equilibrates at its critical value, $\Delta w_{\text{critical}}$. From Eq. (3.3) it is clear that the heat fluxes, Π_1 and Π_2, must balance the excess of $\Delta\Theta^*$ over $\Delta\Theta^*_{\text{critical}}$. The following balances are found to hold in the equilibrated (steady) state:

$$\frac{\sigma_0 \Delta w_{\text{critical}}}{h''} = \Delta\Theta^*_{\text{critical}} - \Delta\Theta_{\text{critical}}. \quad (3.4)$$

$$\frac{\Pi_1}{h''} + \frac{\Pi_2}{h''} = \Delta\Theta^* - \Delta\Theta^*_{\text{critical}}. \quad (3.5)$$

This behavior is shown in Fig. 1 for $n = 1.3$. The solid portion of the line marked "HADLEY" denotes a stable basic state; the dashed portion denotes an unstable basic state. As $\Delta\Theta^*$ is increased from zero (note: $\Delta\Theta^* = 2\sqrt{2}\theta^*_A$), the mean temperature difference, $\Delta\Theta$, increases linearly with the forcing and satisfies the Hadley solution (3.1–3.2). At the critical $\Delta\Theta^*$, this behavior ceases as the basic state becomes baroclinically unstable. For values of $\Delta\Theta^*$ beyond $\Delta\Theta^*_{\text{critical}}$, the meridional temperature gradient equilibrates at its neutral level [Eq. (3.4)]. This neutral level is the critical $\Delta\Theta$ for baroclinic instability of the most unstable wave (zonal wavenumber 2). The vertical velocity, Δw, is observed to have a similar behavior, but is not plotted because its amplitude is very small. It is the heat flux due to wavenumber 2, Π_2, which picks up the excess of $\Delta\Theta^*$ above its critical value, $\Delta\Theta^*_{\text{critical}}$ [Eq. (3.5)]. Wavenumber 2, which is more unstable, extracts available potential energy from the mean flow and lowers the meridional temperature gradient to its critical value (which is lower than the critical value for baroclinic instability of wavenumber 1), thus causing the wavenumber 1 disturbance to decay. Because the model is quasi-linear, there are no direct interactions between wavenumbers 1 and 2, and therefore there is no other channel through which wavenumber 1 can grow. All of the heat flux is transported by wavenumber 2 (i.e., $\Pi_1 \equiv 0$, $\Pi_2 \neq 0$).

If, on the other hand, the basic state is perturbed with only a wavenumber 1 perturbation (i.e., with the initial amplitude of wavenumber 2 set to zero) the result is Fig. 2. The model now equilibrates at $\Delta\Theta^*_{\text{critical}}$ of the more stable wavenumber 1. This equilibration is supercritical with respect to wavenumber 2, but neutral with respect to wavenumber 1. Since there is no way for wavenumber 2 to extract energy from the system, it remains unexcited. All of the heat flux is accomplished by wavenumber 1 (i.e., $\Pi_1 \neq 0$, $\Pi_2 \equiv 0$). This is similar to nonlinear baroclinic adjustment (to be discussed next), in that when there is some mechanism preventing the more unstable wave from extracting energy from the mean flow, the temperature gradient is then maintained by the next (less) unstable wave at its critical value.

4. Nonlinear baroclinic adjustment

We now turn our attention to the fully nonlinear model which allows waves of different scales to interact. The question we wish to address is: how will nonlinear interactions among the various scales alter the behavior observed in the above quasi-linear model? In nonlinear two-layer models, supercritical meridional temperature gradients have been observed (e.g., Salmon 1980; Vallis and Roads 1984). This is in contrast to the results obtained in simplified two-layer models such as the one described above. In this section we will describe the mechanism governing the supercritical equilibration of the meridional temperature gradient.

a. The linear baroclinic stability problem

The linear stability problem provides important information for understanding the relation between the nonlinear equilibration mechanism and the quasi-linear baroclinic adjustment process. It is a straightforward matter to show that for a nonconstant basic state, the coefficients of the perturbation equation will not be constant. In the present model the basic state is described by

$$\Psi = \psi_A \sqrt{2}\cos(y)$$
$$\Theta = \theta_A \sqrt{2}\cos(y).$$

Perturbing the governing equations about this state yields

$$\frac{\partial}{\partial t}\nabla^2\psi' = -\psi_A\sqrt{2}\sin(y)\left(\frac{\partial}{\partial x}\nabla^2\psi' + \frac{\partial\psi'}{\partial x}\right) - \theta_A\sqrt{2}\sin(y)\left(\frac{\partial}{\partial x}\nabla^2\theta' + \frac{\partial\theta'}{\partial x}\right)$$
$$- \beta_0\frac{\partial\psi'}{\partial x} - \nu\nabla^2(\psi' - \tau') + \nu_s\nabla^4(\psi' - \tau') \quad (4.1)$$

and

$$\frac{\partial}{\partial t}(\nabla^2\theta' - \alpha\theta') = -\psi_A\sqrt{2}\sin(y)\left(\frac{\partial}{\partial x}(\nabla^2\theta' - \alpha\theta') + \frac{\partial\theta'}{\partial x}\right) - \theta_A\sqrt{2}\sin(y)\left(\frac{\partial}{\partial x}\nabla^2\psi' + (1+\alpha)\frac{\partial\theta}{\partial x}\right)$$
$$- \beta_0\frac{\partial\theta'}{\partial x} + \alpha h''\theta' + \nu\nabla^2(\psi' - \tau') - \nu_s\nabla^4(\psi' - \tau') \quad (4.2)$$

where $\alpha = 2f_0/\sigma_0$.

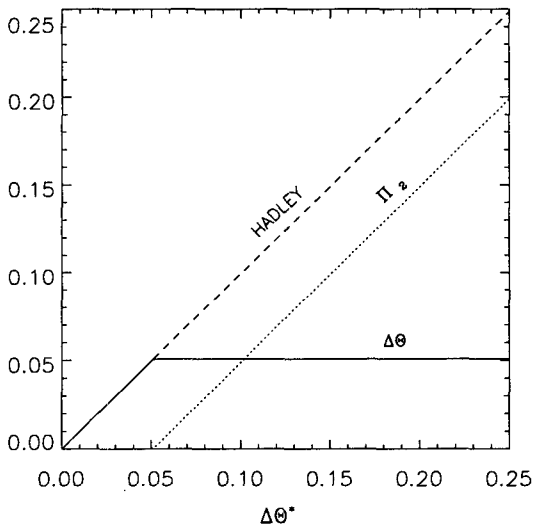

FIG. 1. The Hadley solution, temperature difference ($\Delta\Theta$), and heat flux difference (Π_2) vs thermal driving ($\Delta\Theta^*$) for the ($2x$, $1y$) model for $n = 1.3$. The dashed portion of the Hadley solution represents unstable basic states. (The model truncation used was $X_T = 2$, $Y_T = 1$.)

The eigenvalue problem can be solved by assuming a solution of the form

$$\psi' = \phi(y)\,\exp ik(x - ct)$$
$$\theta' = \gamma(y)\,\exp ik(x - ct). \qquad (4.3)$$

Alternatively, in keeping with the spectral formulation of the present model (2.5), we can assume a solution of the form

$$\psi' = \sum_{j=1}^{Y_T} (\phi_{A(j)} f_{A(j)} + \phi_{K(1,j)} + \phi_{L(1,j)} f_{L(1,j)}) \times \exp(ikct)$$

$$\theta' = \sum_{j=1}^{YT} (\gamma_{A(j)} f_{A(j)} + \gamma_{K(1,j)} f_{K(1,j)} + \gamma_{L(1,j)} f_{L(1,j)}) \times \exp(ikct). \qquad (4.4)$$

In effect, $\phi(y)$ and $\gamma(y)$ have been expanded in Fourier series, which are truncated at wavenumber Y_T. Note that because the coefficients of the perturbation equations (4.1)–(4.2) are functions of y, $\cos(my)$ and $\sin(my)$ are not solutions, as has been assumed by other authors (Reinhold 1989; O'Brien and Branscome 1988). In effect, they assumed the solution to be a superposition of "solutions" of the form:

$$\psi' = \phi_{A_m} \sin(my)\,\exp ik(x - c_m t)$$
$$\theta' = \theta_{A_m} \sin(my)\,\exp ik(x - c_m t). \qquad (4.5)$$

Note that (4.3) and (4.4) are not equivalent to (4.5). Equation (4.4) is not a superposition of solutions; it is a Fourier expansion of the solution.

Figure 3 shows the marginal stability curve for $Y_T = 9$. (Because of the addition rules among the various modes, the results depend on the number of odd y modes. Thus $Y_T = 10$ yields the same result as $Y_T = 9$.) In the remainder of this work, we will use a ($10x$, $10y$) fully nonlinear model and refer back to Fig. 3, with regard to the linear stability of the problem. By varying the horizontal aspect ratio, n, we will change the number of linearly, baroclinically unstable zonal waves present in the model, and show how this affects the equilibration process. Recall that the unstable waves are those for which kn, $k = 1, 2, \cdots$, falls within the marginal curve, for a given driving, as measured by $\Delta\Theta^*$. For clarity, Table 1 shows three values of n, the unstable zonal wavenumbers, and their critical drivings.

b. *Nonlinear baroclinic adjustment in the case where two baroclinic zonal waves are linearly unstable*

The first case we will describe is the case where $n = 1.3$. For this choice of n there are two baroclinically unstable zonal waves, $k = 1, 2$. From Fig. 3 and Table 1 it is clear that wavenumber 2 is the more unstable of the two waves, in the sense that it becomes unstable at a lower driving.

Time integrations of the fully nonlinear ($10x$, $10y$) model were performed for values of thermal driving from $\Delta\Theta^* = 0$ to 0.566, corresponding to a temperature difference across the channel of 0 to 256 K, at radiative equilibrium. It took approximately 500 time steps for the transients to decay and the mean flow to equilibrate (see Fig. 4). The model equations were integrated for 1500 to 2000 time steps (each time step is $f_0^{-1} = 2.8$ h). The zonal mean temperature differences across the channel were averaged using a 30-day running time mean of the last 500 time steps. The results are pre-

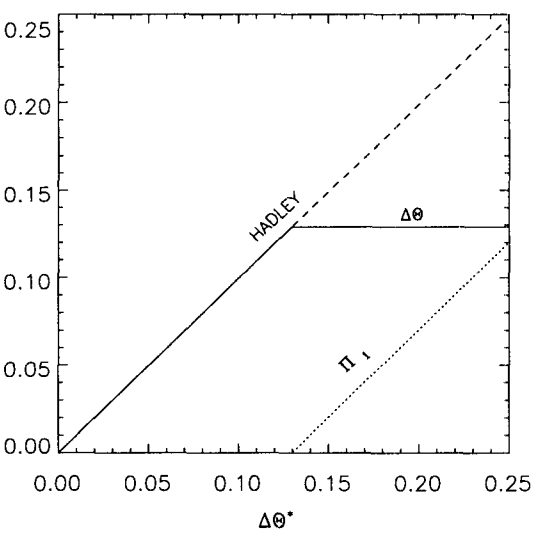

FIG. 2. As in Fig. 1 except that the dotted line is now Π_1, the heat flux difference due to the $k = 1$ wave.

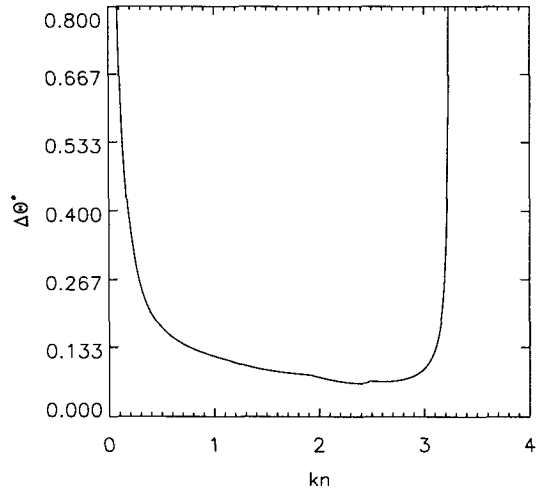

FIG. 3. Marginal curve for the $(1x, 9y)$ model. The unstable region lies inside the marginal curve. Here k is the zonal wavenumber, $k = 1, 2, \cdots$, and n is the horizontal aspect ratio, $n = 2L_y/L_x$, which defines the fundamental zonal harmonic for the model.

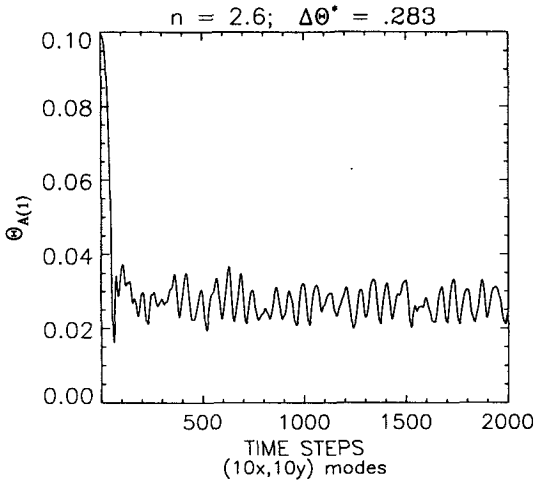

FIG. 4. Time series of $\theta_A(1)$ from the $(10x, 10y)$ model with $n = 1.3$ and $\Delta\Theta^* = 0.283$.

sented in Fig. 5, where the temperature difference, $\Delta\Theta$, is plotted against thermal driving, $\Delta\Theta^*$. The diagonal line is the basic-state Hadley solution (i.e., the radiative equilibrium solution), with the solid and dashed portions denoting stable and unstable states, respectively. The horizontal lines mark the critical temperature differences for linear baroclinic instability of wavenumber 2 (lower line) and wavenumber 1 (upper line). The diamond and "error bar" markings show the averaged, time-dependent results. The bars mark the ranges within which the averaged results lie, and the diamond symbols mark points where the ranges were too small to plot.

As we follow the progression of $\Delta\Theta$ as a function of driving, we see a markedly different type of behavior than was observed in the quasi-linear model. Due to the choice of $n = 1.3$ in both models, the basic state solution becomes unstable at the critical $\Delta\Theta^*$ of wavenumber 2. However, in contrast to the quasi-linear model, the equilibrated zonal temperature difference of the fully nonlinear model *increases* with driving. (Note: "equilibration" here refers to the level at which the time-dependent solution settles, for a given driving.) Although the equilibrated temperature difference is less than that at radiative equilibrium, it clearly is not at the critical value predicted by linear theory. Instead, what is observed is that for very strong forcing, the temperature difference equilibrates at a level *supercritical* to the linearly most unstable wave, but *near the critical* $\Delta\Theta$ of the larger-scale, more stable wavenumber 1.

TABLE 1. Baroclinically unstable waves and their critical drivings for $n = 1.3, 0.82, 0.65$. (k is the zonal wavenumber, $k = 1, 2, \cdots$.)

n	k	$\Delta\Theta^*_{\text{critical}}$
1.3	1	0.09840
	2	0.06780
0.82	1	0.12832
	2	0.08581
	3	0.06602
0.65	1	0.14558
	2	0.09840
	3	0.07863
	4	0.06780

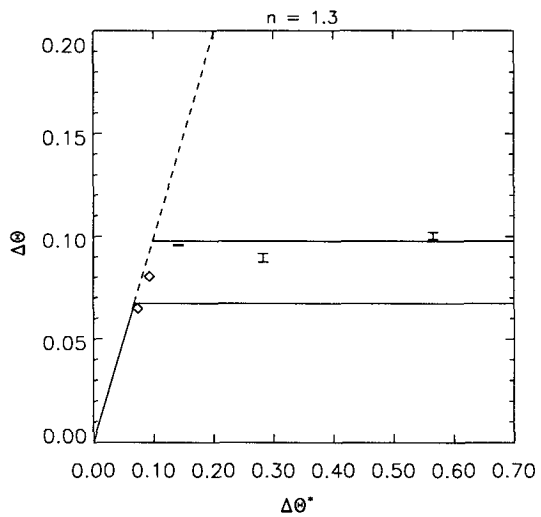

FIG. 5. Temperature difference ($\Delta\Theta$) vs thermal driving ($\Delta\Theta^*$) for the $(10x, 10y)$ model for $n = 1.3$. The diagonal line is the basic-state Hadley solution (i.e., the radiative equilibrium solution), with the solid and dashed portions denoting stable and unstable states, respectively. The horizontal lines mark the critical temperature gradients for linear baroclinic instability of the $k = 2$ wave (lower line) and the $k = 1$ wave (upper line). The diamond and error bar markings show the averaged, time-dependent results.

We further note that this equilibration process is accompanied by a marked growth of the largest-scale wave and a concurrent saturation of the smaller-scale, linearly more unstable wave (Fig. 6). At supercritical but moderate forcing ($\Delta\Theta^* = 0.074, 0.093$), the smaller-scale wavenumber 2 has the greatest amplitude. As the forcing is increased, nonlinear interactions cause wavenumber 2 to saturate. (Compare this result with the quasi-linear case in Fig. 1.) Thereafter, the larger-scale wavenumber 1 continues to increase with forcing. (In Fig. 6 we plotted only the mean streamfunction amplitudes $\psi_{K(k,j)}$ for $k = 1, 2, 3, 4$ and $j = 1$. In all cases, the $j = 1$ components are the ones with the greatest amplitudes.) Note that for this choice of n, wavenumbers 3 and 4 are baroclinically stable, and their amplitudes remain negligible.

The largest-scale wave achieves its growth mainly through wave–mean flow interactions, and, to a much lesser extent, through wave–wave interactions (i.e., upscale cascades). Klein and Pedloskey (1986) also found this to be the case in a two-layer f-plane channel model. Figure 7, row 1 shows results from the fully nonlinear model, while row 2 shows results from a model in which wavenumber 1 was not allowed to extract energy from the mean flow. (In the latter case, wavenumber 1 was still allowed to modify the mean flow.) A comparison of these two rows clearly shows that wavenumber 1 gets almost all of its energy directly from the mean flow. When this interaction is suppressed, the amplitude of wavenumber 1 is negligible. The fact that even in the fully nonlinear case this wave gets most of its energy from wave–mean flow interaction explains why its time series behaves so regularly (similar to the simple quasi-linear case described earlier), and ironically this is especially true for larger wave amplitudes and stronger driving.

This dominance of larger-scale waves is also reflected in the heat flux. Consider the zonally averaged energy equation:

$$\sum_i \frac{\partial}{\partial t}\theta_{A(i)}(t)f_{A(i)} = -n\sum_i\sum_l\sum_m c_{ilm}\psi_l\theta_m f_{A(i)} - \sum_i(\sigma_0\omega_{A(i)} + h''(\theta^*_{A(i)} - \theta_{A(i)}))f_{A(i)}.$$

Here, the subscripts l, m refer to the wave variables—e.g., $\psi_{K(k,j)}$, $\theta_{K(k,j)}$.)—and c_{ilm} are interaction coefficients (see Cehelsky and Tung 1987). If we take the difference of this equation across the channel, we obtain

$$\frac{\partial}{\partial t}\Delta\Theta = \Pi - \sigma_0\Delta w + h''(\Delta\Theta^* - \Delta\Theta),$$

where $\Delta\Theta$ is the zonal-mean temperature difference across the channel (see Fig 5) and Π is the heat flux difference across the channel. The time-averaged heat flux difference is plotted in Fig. 8, as a function of driving. The curves are labeled according to the heat flux carried by the respective wave, and "TOTAL" refers to the total heat flux. (The waves not shown do not contribute significantly to the heat flux. This can be verified by adding the contributions from the waves plotted, and comparing the sum to the curve labeled "TOTAL.")

At relatively low supercritical driving, most of the heat is transported by the more unstable wavenumber 2. However, Fig. 8 clearly shows that for large driving, the more stable, larger-scale wave transports most of the heat needed to maintain the equilibrated state. Indeed, the heat flux due to wavenumber 2 does not increase for $\Delta\Theta^* > 0.283$. Therefore, this wave cannot participate in the baroclinic adjustment process for larger driving. It is therefore not surprising that the temperature gradient has equilibrated near the critical gradient for baroclinic instability of wavenumber 1. This is the mechanism of *nonlinear baroclinic adjustment.* As the driving is increased, nonlinear interactions act in such a way as to allow the larger-scale wave to extract energy from the mean flow, while causing the smaller-scale, linearly more unstable waves to saturate. The temperature gradient equilibrates near the (linear) critical gradient of the main heat-transporting eddy. The scale of this "main heat-transporting eddy" increases with increasing driving. Thus, at large driving the equilibrated gradient becomes supercritical with respect to the linearly most unstable wave, but is nevertheless still near critical with respect to a larger-scale wave, which now becomes the main heat-transporting eddy.

This adjustment process is *quasi-linear* in that it is mainly the interaction between the largest-scale wave and the mean flow that determines the equilibrated state. However, it is inherently a *nonlinear* process because the saturation of the smaller-scale, more unstable wave and the dominance of the largest-scale wave are the result of nonlinear dynamics. Again, the nonlinear dynamics merely determine which wave is the main heat-transporting one. The adjustment process is essentially the same as in the quasi-linear case envisaged by Stone (1978), except with the "linearly most unstable wave" replaced by the "most efficient heat-transporting wave."

c. *Nonlinear baroclinic adjustment in the case where several baroclinic waves are unstable*

The nonlinear baroclinic adjustment mechanism is most clearly illustrated in the above case with two baroclinically unstable zonal waves. In this section we will explore two other cases, one with three ($n = 0.82$) and one with four ($n = 0.65$) unstable waves (see Table 1).

1) THE $N = 0.82$ CASE: THREE UNSTABLE ZONAL WAVES

Figure 9 shows the averaged zonal mean temperature differences across the channel for the $n = 0.82$ case. Again we see a similar behavior as was observed in Fig.

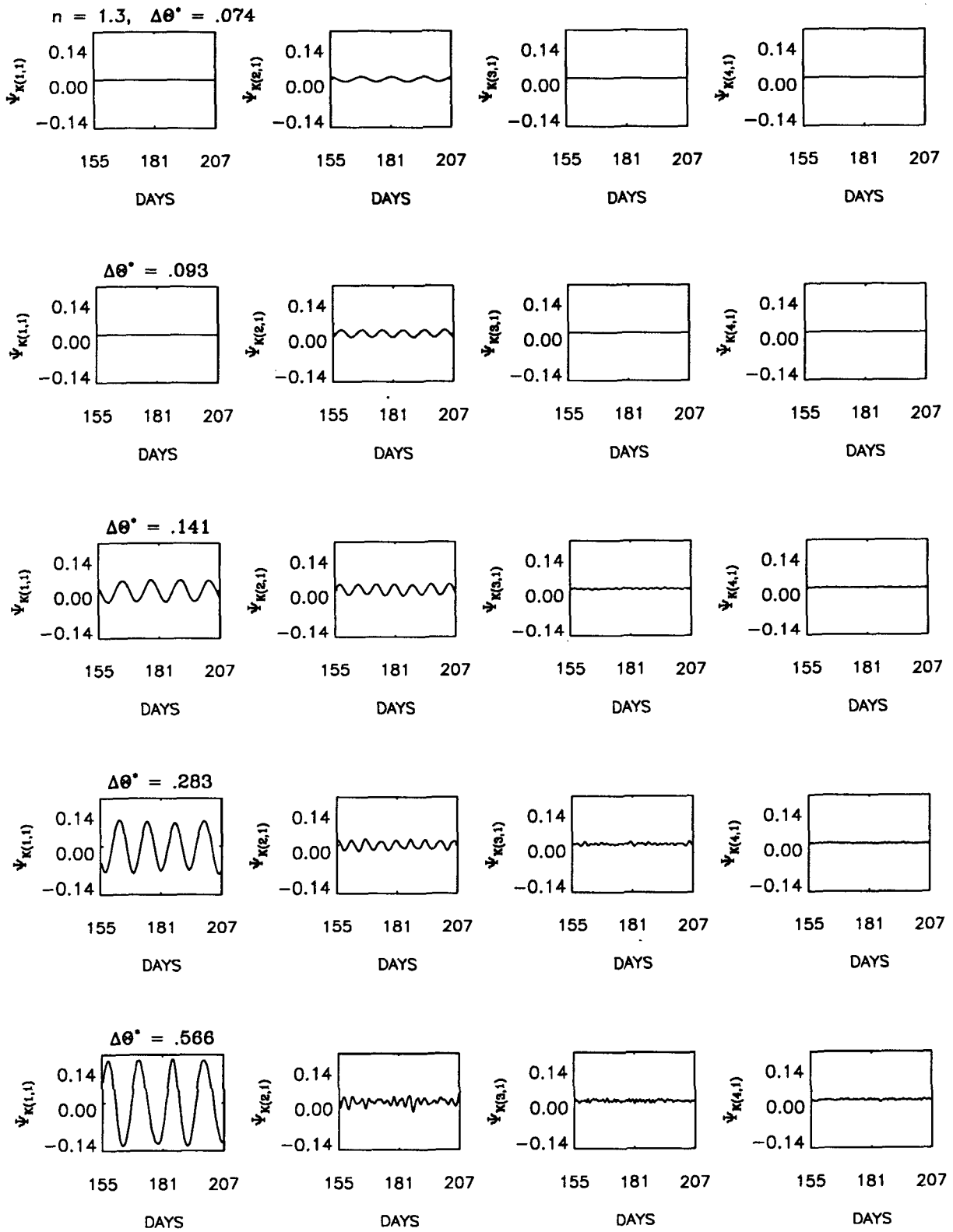

FIG. 6. Time evolution of the components, from left to right, $\psi_{K(1,1)}$, $\psi_{K(2,1)}$, $\psi_{K(3,1)}$ and $\psi_{K(4,1)}$ from the $n = 1.3$, $(10x, 10y)$ model for several values of thermal driving. Row 1: $\Delta\Theta^* = 0.074$; Row 2: $\Delta\Theta^* = 0.093$; Row 3: $\Delta\Theta^* = 0.141$; Row 4: $\Delta\Theta^* = 0.283$; Row 5: $\Delta\Theta^* = 0.566$.

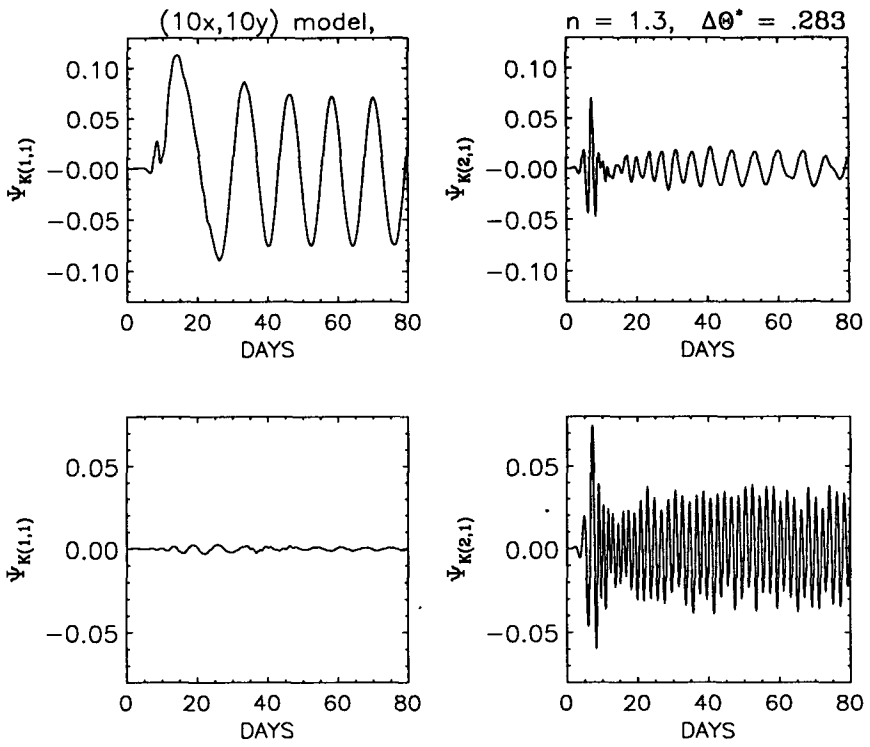

FIG. 7. Time evolution of amplitudes, from left to right, $\psi_{K(1,1)}$ and $\psi_{K(2,1)}$ for the $n = 1.3$, $(10x, 10y)$ model, $\Delta\Theta^* = 0.283$. Row 1: The full model; Row 2: Interactions which allow wave 1 to be modified by the mean flow have been suppressed.

5 for the two-wave case. The temperature difference, $\Delta\Theta$, increases with driving but tapers off near the critical $\Delta\Theta$ for baroclinic instability of the largest-scale wave. As the driving is increased, successively larger-scale waves become dominant in transporting the heat needed to maintain the equilibrated state (see Fig. 10). For example, at $\Delta\Theta^* = 0.141$, wavenumber 2 contributes the most to the heat flux, and the equilibrated $\Delta\Theta$ is near the critical $\Delta\Theta$ for wavenumber 2. At $\Delta\Theta^* = 0.283$, wavenumbers 1 and 2 transport almost equal

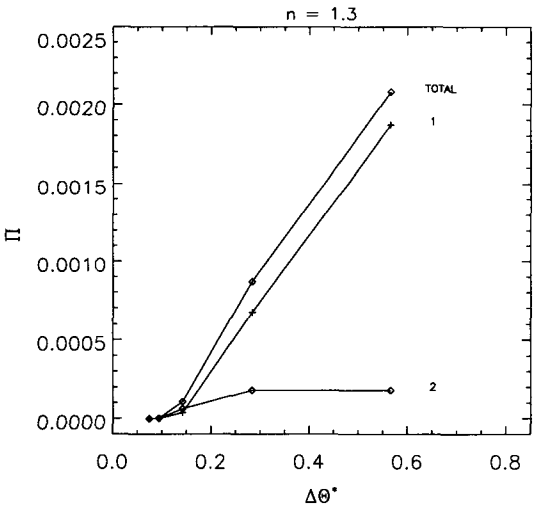

FIG. 8. Heat flux difference across the channel (Π) vs $\Delta\Theta^*$ for the $n = 1.3$, $(10x, 10y)$ model. The numbered curves show Π due to the respective wave scale, and "TOTAL" shows the total contribution from all waves.

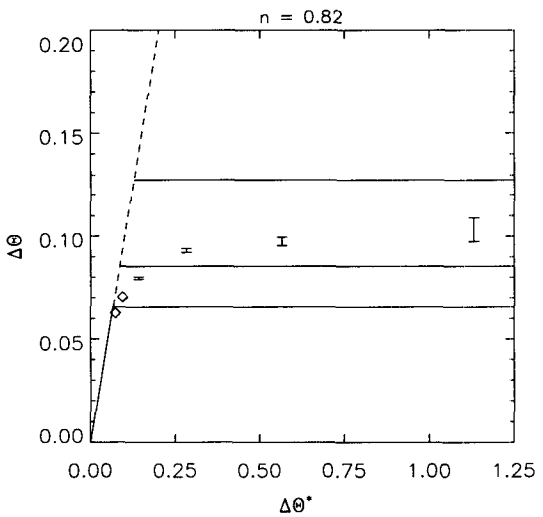

FIG. 9. As in Fig. 5, but for $n = 0.82$. The horizontal lines from bottom to top are the critical $\Delta\Theta$ of the $k = 3$, $k = 2$, and $k = 1$ waves, respectively.

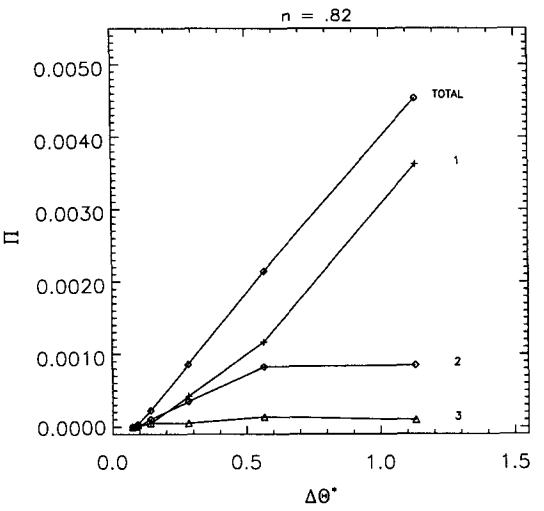

FIG. 10. As in Fig. 8, but for $n = 0.82$.

amounts of heat. By $\Delta\Theta^* = 0.566$ the contribution of wavenumber 1 to the heat flux is much greater than that of all other waves. While energy is cascading to ever larger scales, the smaller-scale, more unstable waves are saturating. This is clearly seen in Fig. 10 where the heat fluxes of the smaller-scale wavenumbers 2 and 3 taper off and reach their maxima, while that of the largest-scale wavenumber 1 continues to increase with driving.

This saturation effect is also evident in the wave amplitudes themselves (Fig. 11). At $\Delta\Theta^* = 0.74$, wavenumber 3 is dominant, while at $\Delta\Theta^* = 0.093$, wavenumbers 2 and 3 have comparable amplitudes. By the time $\Delta\Theta^*$ reaches 0.141, wavenumber 2 is dominant and contributes most to the heat flux (Fig. 10), while wavenumber 3 has saturated. This process continues so that at very high driving, $\Delta\Theta^* = 0.566$, wavenumber 1 attains the greatest amplitude (Fig. 11) and transports most of the heat (Fig. 10), while all other waves, as well as their heat fluxes, are saturated.

Comparing Figs. 5 and 9, one difference is immediately evident. The increase of $\Delta\Theta$ beyond $\Delta\Theta_{critical}$ of the linearly most unstable wave is steeper for the $n = 1.3$ case. When only two waves in the model are baroclinically unstable, the equilibrated temperature difference does not deviate much from the Hadley solution until the driving is supercritical for the largest-scale wavenumber 1. Thereafter the equilibrated temperature difference remains near the critical value of wavenumber 1. When more than two waves in the model are baroclinically unstable, this behavior is slightly different. Although the equilibrated temperature difference in all cases ($n = 1.3, 0.82, 0.65$) begins to differ significantly from the Hadley solution for drivings supercritical to the largest-scale wave, the climb to $\Delta\Theta_{critical}$ of the largest-scale wave is much more gradual. Thus, in models with several baroclinically unstable waves, it takes a much larger driving for the equilibrated temperature difference to reach $\Delta\Theta_{critical}$ of the largest-scale wave; i.e., it takes more energy to saturate more waves.

In Fig. 9, the equilibrated temperature difference is approaching, but is not yet at the critical $\Delta\Theta$ of wavenumber 1, for the range of driving considered. In this range, $\Delta\Theta$ is still increasing with driving, but very slowly. This is a very promising aspect of the model in terms of predicting the equilibrated temperature difference. The fact that the change in $\Delta\Theta$ is quite small means that for seasonal changes in solar insolation, $\Delta\Theta$ will be approximately constant. For example, in going from $\Delta\Theta^* = 0.283$ to 0.566 (a 64 K temperature difference across the channel at radiative equilibrium), $\Delta\Theta$ changes by approximately only 4% (see Fig. 9). Even for lower, more realistic driving, the equilibrated $\Delta\Theta$ increases more slowly than the radiative equilibrium (i.e., Hadley) solution. A change from $\Delta\Theta^* = 0.141$ to 0.283 (a 32 K temperature difference across the channel at radiative equilibrium) results in an approximately 16% increase in the equilibrated temperature difference. This characteristic of the model atmosphere agrees well with the observed atmosphere. Stone (1978) noted that the observed midlatitudinal temperature gradient remains approximately constant in the course of a year.

2) THE $N = 0.65$ CASE: FOUR UNSTABLE ZONAL WAVES

Figures 12 and 13 show the equilibrated temperature differences and the heat flux differences as functions of driving for $n = 0.65$. The basic features of this case are the same as in the previous two cases ($n = 1.3$ and $n = 0.82$). For $\Delta\Theta^*$ above the critical driving for the largest-scale wave, the equilibrated temperature difference begins to differ significantly from the basic state Hadley solution. Thereafter the increase in $\Delta\Theta$ is much more gradual. The temperature difference, $\Delta\Theta$, eventually approaches the critical $\Delta\Theta$ for linear instability of the largest-scale wave. The heat flux plot (Fig. 13) again shows successively larger-scale waves transporting most of the heat, as the thermal driving increases.

As was pointed out in the $n = 0.82$ case, a much larger driving is required to saturate the heat fluxes of all waves smaller than the largest-scale wave, than in models with fewer baroclinically unstable waves. In the $n = 1.3$ case, the heat flux transported by wavenumber 2 was saturated by $\Delta\Theta^* = 0.283$. In the $n = 0.82$ case, the heat flux carried by wavenumber 3 was saturated by $\Delta\Theta^* = 0.283$, and that carried by wavenumber 2 was saturated by $\Delta\Theta^* = 0.566$. In the $n = 0.65$ case, the heat flux transported by wavenumber 4 was saturated by $\Delta\Theta^* = 0.283$, and that transported by wavenumber 3 saturated by $\Delta\Theta^* = 0.566$. However, we see that the heat flux carried by wavenumber 2 has not yet saturated at $\Delta\Theta^* = 0.566$. This saturation effect is also evident in the wave amplitudes (see Fig. 14). We thus see that the addition of baroclinically unstable waves makes the cascade to larger scales less efficient.

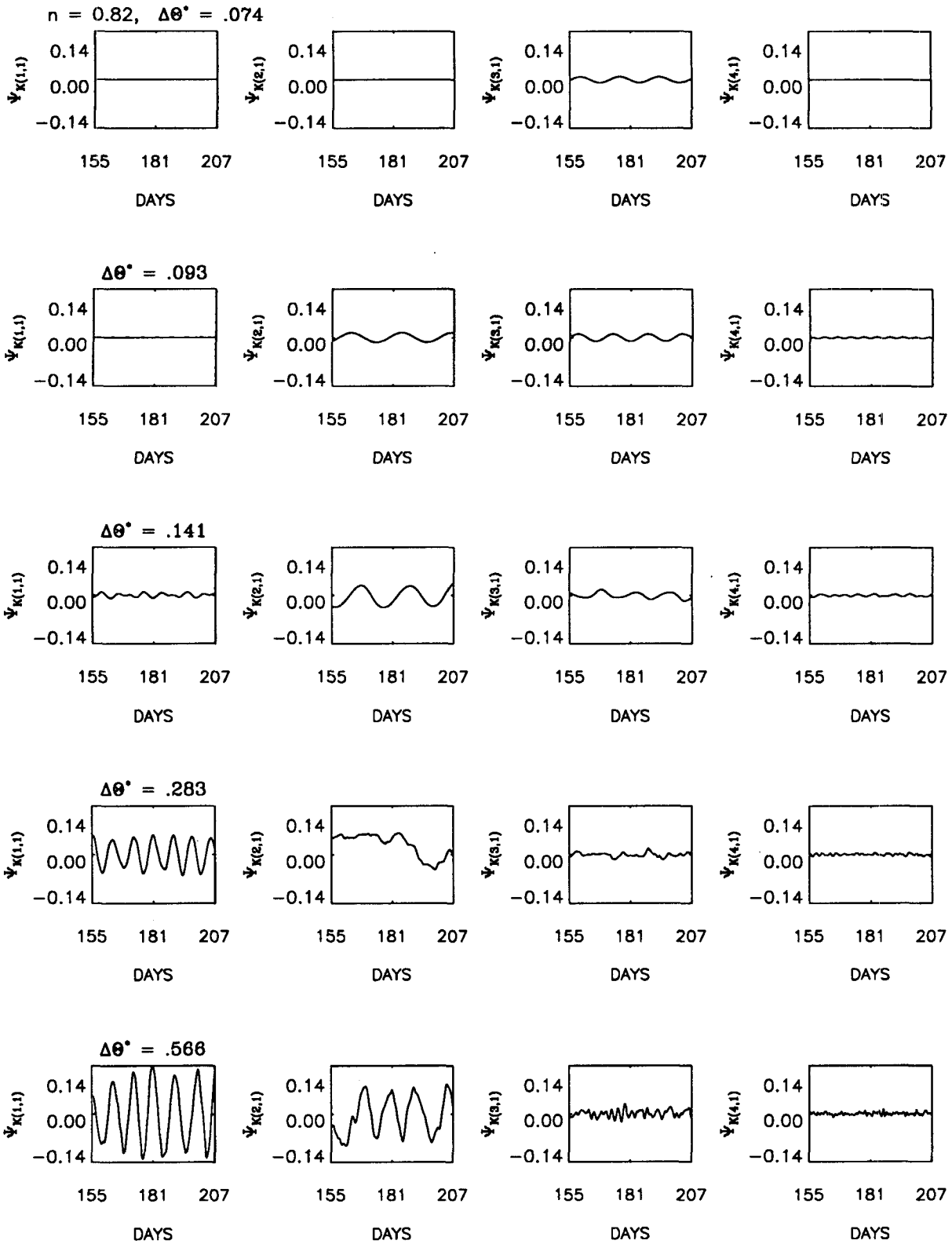

FIG. 11. As in Fig. 6, but for $n = 0.82$.

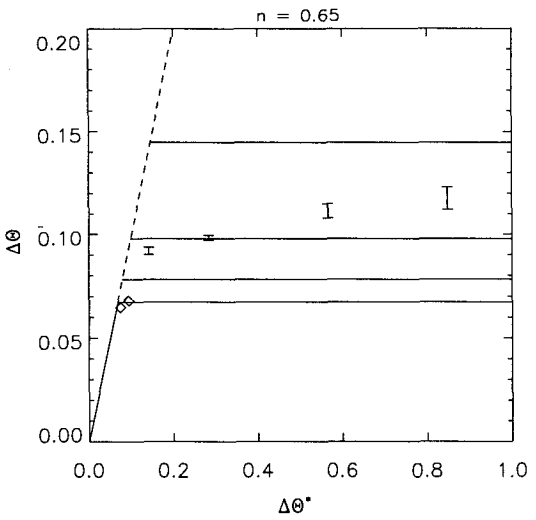

FIG. 12. As in Fig. 5, but for $n = 0.65$. The horizontal lines from bottom to top are the critical $\Delta\Theta$ of the $k = 4$, $k = 3$, $k = 2$, and $k = 1$ waves, respectively.

This case ($n = 0.65$) is particularly well suited for comparisons with the $n = 1.3$ case, because two of the baroclinically unstable waves of the former have exactly the same scale as the baroclinically unstable waves of the $n = 1.3$ case. More precisely, the $n = 1.3$ wavenumber 1 has a nondimensional zonal length of $1n = 1.3$, which is the same as that of the $n = 0.65$ wavenumber 2, with $2n = 1.3$. Likewise, the $n = 1.3$ wavenumber 2 has the nondimensional length $2n = 2.6$, which corresponds exactly to the $n = 0.65$ wavenumber 4, with $4n = 2.6$. We will next compare the behaviors of these waves in the two models.

Perhaps the most striking comparison between the two models concerns the behaviors of the $n = 1.3$ wavenumber 1 with the $n = 0.65$ wavenumber 2. A look at Figs. 8 and 13 shows that the heat flux transported by the former does not saturate, while that transported by the latter does. The largest-scale waves in these models (e.g., the $n = 1.3$ wavenumber 1) are not subject to the same mechanism of saturation as the smaller-scale waves. These waves and their heat fluxes continue to grow with driving (Figs. 6 and 8, 10 and 11, 13 and 14), long after all other waves have saturated.

It is important to point out that the waves with the greatest amplitudes are not necessarily the main heat-transporting eddies. For example, at $\Delta\Theta^* = 0.141$, wavenumber 3 transports most of the heat (Fig. 13), but its amplitude is smaller than that of wavenumber 2 (Fig. 14). Likewise, at $\Delta\Theta^* = 0.283$, wavenumber 2 transports most of the heat (Fig. 13), but its amplitude is smaller than that of wavenumber 1 (Fig. 14). In general, a larger driving is required for a larger-scale wave to transport the most heat, than for that wave to attain the greatest amplitude. Thus the correlation between the temperature and velocity perturbations is a crucial element here. Perhaps for this reason Rhines' wavenumber criterion (Rhines 1975) for the limit of upscale energy cascades could not be used to predict the equilibrated temperature gradient in our model.

We also ran a case where five zonal waves (wavenumbers 1–5) were baroclinically unstable, with wavenumber 4 being more unstable than wavenumber 5. The results were as in the above $n = 0.82$ and $n = 0.65$ cases. As the driving was increased, successively larger-scale waves became dominant. This case showed that the dominance of more stable waves for higher values of driving necessarily meant the dominance of *larger-scale,* more stable waves.

As a final comment, we would like to add that our results appear to be consistent with those of Salmon (1980, see Table III). In experiments B and C (experiment A concerns the $\beta = 0$ case), Salmon found that the average shear (in our study we use the meridional temperature gradient as a measure of linear baroclinic stability) for a given driving was near the critical shear for the wavenumber of maximum $F(k)$, which may be taken as a measure of the heat flux (k is the wavenumber), and that the latter wavenumber is slightly smaller than that of the linearly most unstable wave. (However, it is not yet at wavenumber 1 for the particular value of driving used.) This appears to be consistent with our findings and suggests that the average shears in Salmon's two experiments had not yet reached the maximum asymptotic value; i.e., that the forcings he used were in an intermediate range.

5. "Exceptions to the rule": quasi-linear versus nonlinear

As mentioned in the Introduction, there are known exceptions to the proposed theory (Vallis 1988; Panetta and Held 1988). However, these mostly involve experiments in which wave–wave interactions are artificially suppressed by truncating all but one zonal wavenumber, while many meridional modes are retained. We shall illustrate the difference between the

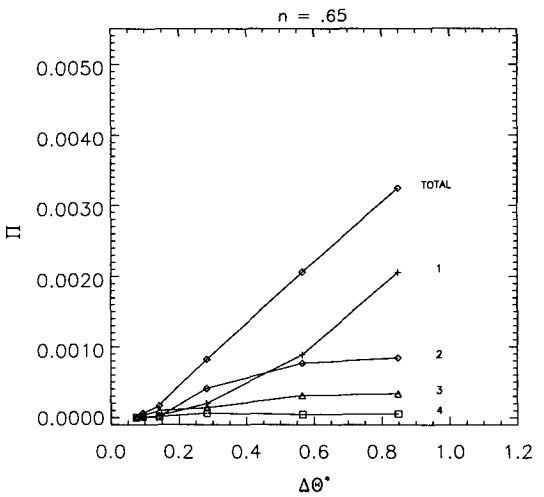

FIG. 13. As in Fig. 8, but for $n = 0.65$.

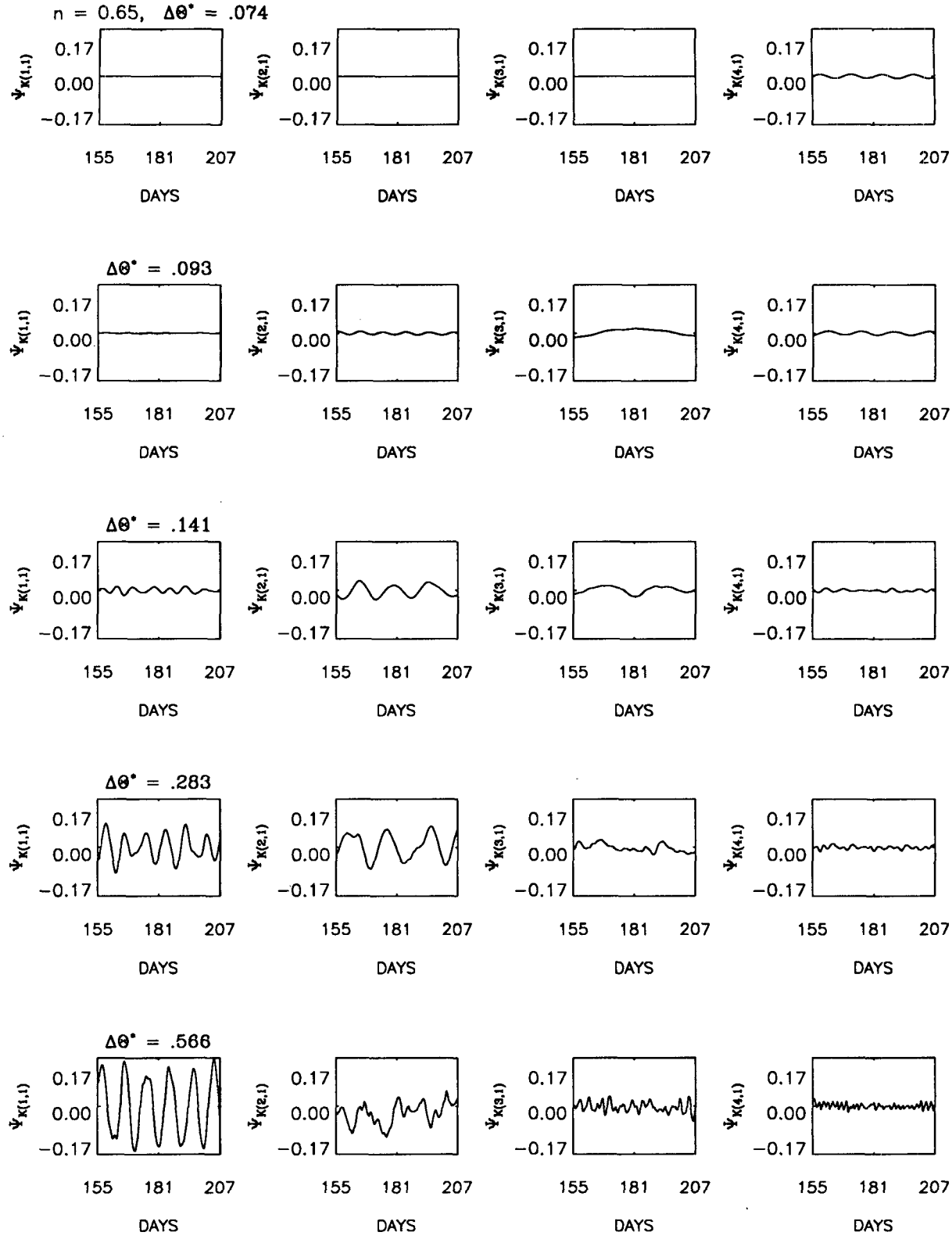

FIG. 14. As in Fig. 6, but for $n = 0.65$.

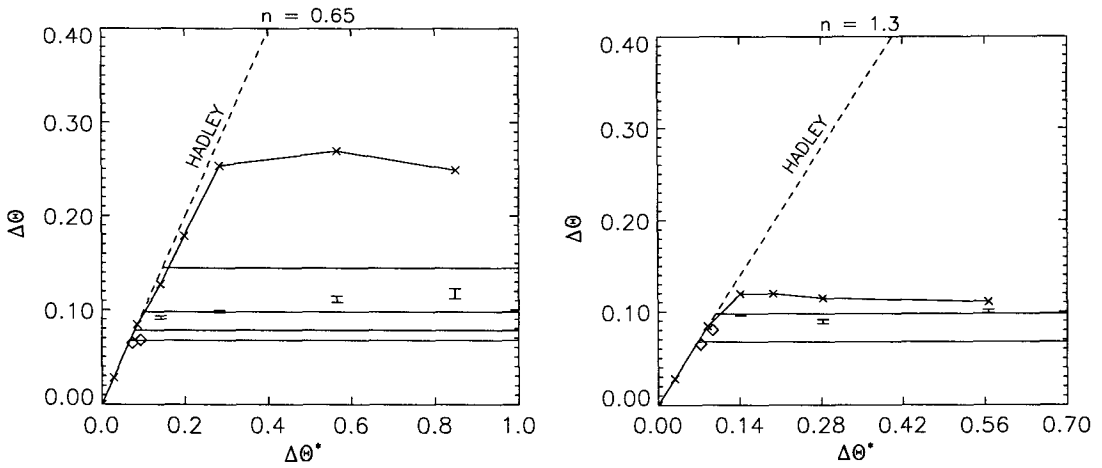

FIG. 15. Temperature difference ($\Delta\Theta$) vs thermal driving ($\Delta\Theta^*$) for the ($1x$, $10y$) and ($10x$, $10y$) models. The "x" marks denote results from the ($1x$, $10y$) model. (a) $n = 0.65$. All other markings are as in Fig. 12. (b) $n = 1.3$. All other markings are as in Fig. 5.

quasi-linear models and our nonlinear model by comparing experiments run with ($1x$, $10y$) and ($10x$, $10y$) truncations of our model.

In the nonlinear case, the scale of the dominant heat-transporting wave is determined by internal dynamics, as discussed in the previous section. In the quasi-linear case, the scale of the sole zonal wave has to be specified. This is accomplished by choosing an appropriate value of the parameter n, and retaining zonal wavenumber 1 in the truncation.

In Fig. 15a, we compare the equilibrated mean temperature difference across the channel as a function of radiative driving for the nonlinear ($10x$, $10y$) and the quasi-linear ($1x$, $10y$) cases for $n = 0.65$. In Fig. 15b the case of $n = 1.3$ is shown. (The results for $n = 0.82$ fall in between these two cases, and are therefore not shown.) For small supercriticality it is seen that the ($1x$, $10y$) model agrees approximately with the ($10x$, $10y$) model when the appropriate wavenumber is chosen.[4] This is to be expected in a "weakly nonlinear" regime. As the driving increases, however, the quasi-linear response begins to deviate from the nonlinear response, with the former achieving "supercritical equilibration," while the latter equilibrates near the critical value of the dominant wave, and eventually (for sufficiently high driving) asymptotes (from below) to the critical value for the largest-scale wave. The fact that the quasi-linear model attains an equilibrated temperature difference that is higher than the critical value even for the longest wave is consistent with the findings of Vallis (1988) and Panetta and Held (1988). Nevertheless, it is not an exception to our proposed theory because this situation results directly from the zonal wave truncation adopted, and is not a property of the fully nonlinear model (Fig. 15). In their study using an f-plane model, Klein and Pedloskey (1986) also found that the zonal harmonies play a crucial role in determining the appropriate correction to the mean flow.

The reason why in a time-dependent calculation the quasi-linear model does not equilibrate near the critical value as predicted by linear instability theory is as follows. The linear instability prediction is based on the preexisting flow. This flow [with a $\sin(y)$ structure for $\bar{u}$, the mean zonal velocity[5]] is modified through wave–mean flow interactions, which introduce a "barotropic shear" (James 1987) with a higher meridional mode structure [mainly $\sin(2y)$ for $\bar{u}$, see Figs. 16a,b]. Such a mean flow is less unstable than the preexisting flow (James 1987). Thus the critical value is higher. The quasi-linear model with sufficient meridional resolution equilibrates at the *critical* value for instability based on the modified flow, but is supercritical to the preexisting flow (Cai 1991, personal communication). Viewed in this light—i.e., when the meridional shear of the basic state is taken into account in linear stability calculations—there does not appear to be any inconsistency between these exceptional cases and Stone's original theory of baroclinic adjustment.

While this modification of the meridional structure of the mean flow by the unstable wave can also occur in the fully nonlinear case, the effect is in most cases less significant. Figures 16c,d show that when several waves are linearly unstable and wave–wave interactions are allowed to take place (i.e., no severe zonal truncation), the barotropic component of the zonal velocity (i.e., the mean zonal velocity of the two layers) retains

[4] For small supercriticality one ought to use quasi-linear models with the appropriate zonal scale (i.e., the appropriate smaller scale, which is equal to the dominant scale in the nonlinear model) for comparisons with nonlinear models. At highly supercritical driving, when the nonlinear model is dominated by the largest-scale wave, a comparison between the quasi-linear model with the largest zonal scale and the nonlinear model is appropriate.

[5] The overbar represents a zonal average.

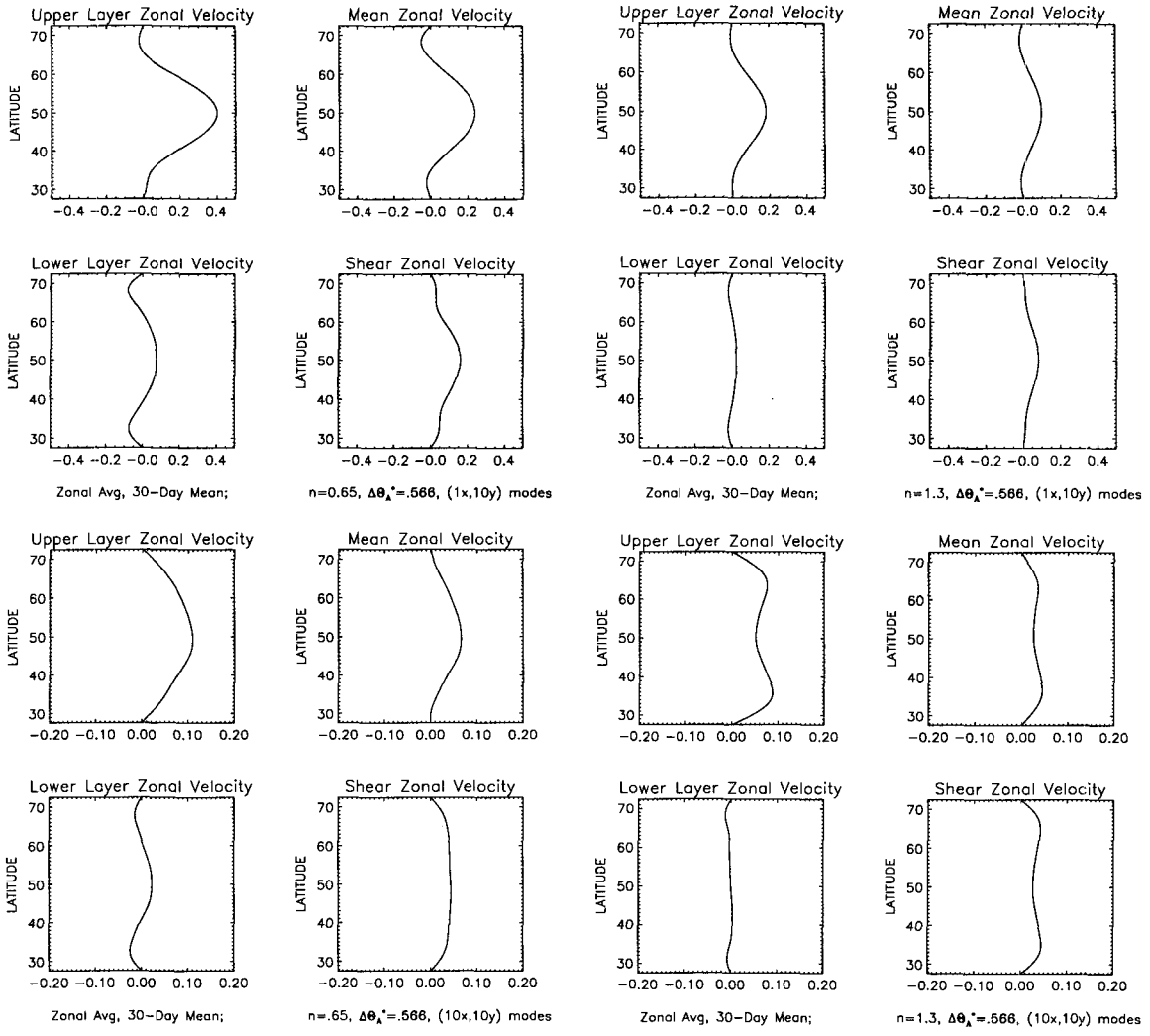

FIG. 16. Meridional structure of zonally averaged, 30-day time-mean zonal velocity. $\Delta\Theta^* = 0.566$: (a) $n = 0.65$, $(1x, 10y)$ model, (b) $n = 1.3$, $(1x, 10y)$ model, (c) $n = 0.65$, $(10x, 10y)$ model, (d) $n = 1.3$, $(10x, 10y)$ model.

its broad preexisting meridional shape [$\sin(y)$ for $\bar{u}$]. This explains why the nonlinear model equilibrates near the critical value based on the preexisting flow, and is true whenever the number of unstable waves is two or more.

As the number of linearly unstable zonal waves is reduced (i.e., as the parameter n is increased in the nonlinear model), the quasi-linear effect mentioned above becomes more pronounced. For $n = 1.3$ (two unstable zonal waves), reduction of the mean zonal flow starts to show in the middle of the channel. For $n = 2.6$ (one unstable zonal wave),[6] the $\sin(2y)$ structure in $\bar{u}$ becomes prominent (see Fig. 17a). In fact, for $n = 2.6$, the $(1x, 10y)$ (Fig. 17b) and the $(10x, 10y)$ (Fig. 17a) models behave very similarly. This is because only one zonal wavenumber is excited in this particular geometry, even though ten zonal waves are allowed. In Fig. 18 we plot the equilibration diagram for both the $(1x, 10y)$ and $(10x, 10y)$ models for the $n = 2.6$ case. The quasi-linear and fully nonlinear equilibrations are almost indistinguishable. This situation, however, is not a property of the more general and more realistic cases. In these cases, several linearly unstable zonal waves are always present, and the nonlinear results deviate from the quasi-linear results. It is ironic to note that it is the quasi-linear equilibration that is always more supercritical than the nonlinear one, based on the preexisting flow.

A more precise but less useful statement of our proposed theory is this: the mean meridional temperature difference equilibrates near the critical value of the main heat-transporting eddy, as predicted by linear stability theory based on the *modified* flow. The scale of the main heat-transporting wave increases with in-

[6] $n = 2.0$ corresponds to the case where the fundamental meridional and zonal wavelengths are equal, and $n > 2.0$ corresponds to a wide channel geometry.

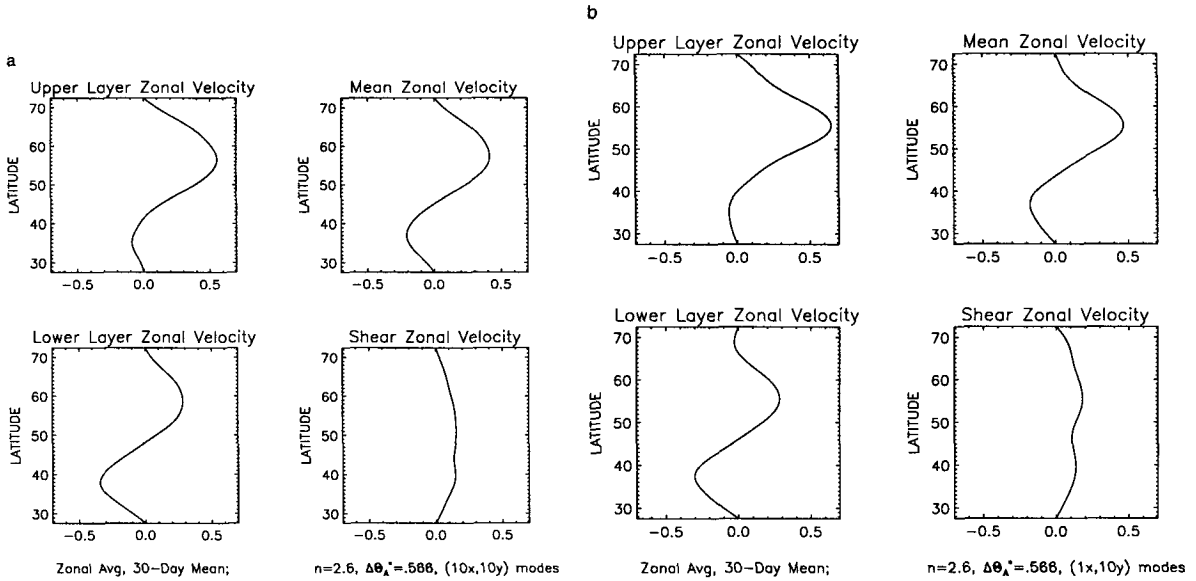

FIG. 17. Meridional structure of zonal velocity: $\Delta\Theta^* = 0.566$, $n = 2.6$, (a) $(10x, 10y)$ model, (b) $(1x, 10y)$ model.

creasing driving. At sufficiently high radiative driving, the equilibrated meridional temperature difference asymptotes to the critical value of the longest wave permitted by the geometry.

If only the *preexisting* flow is known, our proposed theory can be stated as follows: The mean meridional temperature difference equilibrates near the critical value of the main heat-transporting eddy as predicted by linear stability theory based on the preexisting flow, unless the number of linearly unstable zonal waves is severely limited. The rest of the theory remains the same as above.

6. Conclusion

The concept of baroclinic adjustment as proposed originally by Stone (1978) involves essentially a quasi-linear mechanism. When the meridional temperature gradient exceeds the critical value for baroclinic instability of the linearly most unstable wave, that wave will be excited. Its role is to transport enough heat poleward to equilibrate the temperature gradient near this critical value. Thus it is solely the interaction between the most unstable wave and the mean flow that equilibrates the meridional temperature gradient near the level predicted by linear theory.

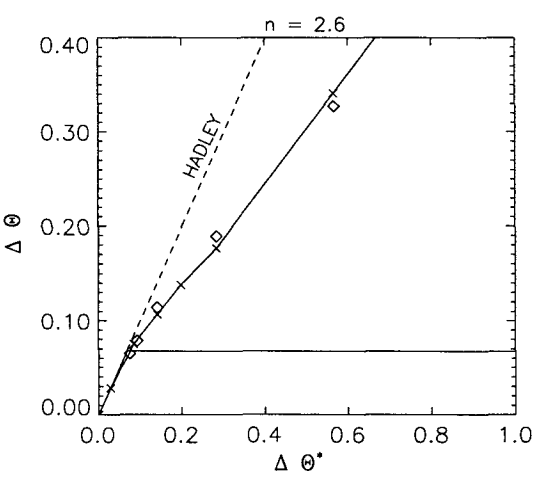

FIG. 18. As in Fig. 15, but for $n = 2.6$.

In fully nonlinear models, supercritical (i.e., supercritical with respect to the most unstable wave) temperature gradients were reported, and the baroclinic adjustment mechanism was thought to be no longer valid. Both observations and numerical modeling show that the main heat-transporting eddies have scales larger than the baroclinically most unstable waves. Nevertheless, the model temperature gradient does equilibrate. What needs to be addressed is to what this equilibrated temperature gradient is quantitatively related. We have related the supercritical temperature gradients observed in our nonlinear model to the critical gradients for baroclinic instability of the main heat-transporting eddies. Thus, our proposed *nonlinear baroclinic adjustment* mechanism also has a quasi-linear nature. The interaction between the main heat-transporting eddies and the mean flow equilibrates the temperature gradient near the critical gradients of those eddies. The scale of the wave responsible for most of the heat transport increases with driving.

Yet nonlinear baroclinic adjustment is fundamentally a nonlinear process. It crucially depends on wave–wave interactions to saturate the smaller-scale waves. Nonlinear baroclinic adjustment can thus be viewed as having two aspects: 1) *nonlinear*—the dominance of larger-scale waves and the saturation of the smaller-scale waves and 2) *quasi-linear*—the equilibration of the meridional temperature gradient by the main heat-

transporting eddies through wave–mean flow interaction.

Previous studies (Salmon 1980; Vallis 1988) reported that the meridional temperature gradient (or, equivalently, the vertical shear of the mean wind) was supercritical. Therefore, it was concluded that there was no maximum level at which it equilibrated. The reason why this asymptotic value of the equilibrated temperature gradient was not observed is that only one value of forcing was used for a given set of parameters. Under such conditions it is not possible to observe the behavior of the equilibrated temperature gradient as a function of forcing. What was observed was only that quasi-linear baroclinic adjustment did not hold because of the existence of a "supercritical" temperature gradient.

The proposed nonlinear baroclinic adjustment mechanism was also found to hold in a case with very high damping (see Cehelsky 1987; Cehelsky and Tung 1987, Fig. 15). This process of equilibration appears to be a robust feature of nonlinear dynamics that is not sensitive to changes in parameter values.

Since we have not studied all parameter regimes, we do not know how generally applicable our result is. However, all known exceptions to our proposed mechanism can be accounted for by noting that they are mostly the results of artificial suppression of nonlinear wave–wave interactions.

We also do not know how applicable our result is to the real atmosphere, since it is based on a two-layer channel model. Nevertheless, some inferences can be made. Since the baroclinically most unstable wave in the atmosphere occurs at around zonal wavenumber 12, the radiative driving has to be extremely high before zonal wavenumbers 12, 11, 10, 9, 8, etc. can be saturated. (Recall that in our model, in the cases with more unstable zonal wavenumbers, it took considerably higher driving to saturate the smaller-scale waves. Contrast, for example, Figs. 5 and 12.) Therefore, it is likely that under the present radiative driving, the equilibrated temperature gradient is not yet at the asymptotic value with wavenumber 1 being the most efficient heat-transporting eddy. In other words, the radiative driving may be in the "intermediate range" discussed in this paper. Our result can still be used to explain why the observed temperature gradient is fairly insensitive to large changes in radiative input via the baroclinic adjustment process.

A central premise of the theory of baroclinic adjustment is that the model atmosphere attempts to maintain a temperature gradient neutral to baroclinic instability, and that the transient heat fluxes due to self-excited waves are whatever is necessary to achieve this state. It then follows that the process is independent of whether topographic forcing or oceanic heat transport are present. Preliminary calculations using our model show that this is indeed the case (see Cehelsky 1987; Cehelsky and Tung 1987). Our calculations agree with the observations of Stone and Miller (1980, section 3c), who found that the stationary and transient heat fluxes have a strong negative feedback. The two vary in a complementary way, so that it is the *total* heat flux that is correlated with the mean temperature gradient.

Acknowledgments. This research was supported by the National Science Foundation, Atmospheric Sciences Division, under Grants ATM-89003340 and ATM-8606268. PC acknowledges support from the MIT–Japan Science and Technology Program, and computational support from the Geophysical Institute, University of Tokyo. While at COLA during the final revision of the manuscript, PC was supported by ATM-8719167. PC would like to thank Taroh Matsuno and KKT would like to thank Peter Stone for their helpful comments and encouragement. We are grateful to the editor, Isaac Held, and to the reviewers for their insightful comments.

REFERENCES

Boer, G. J., and T. G. Shepard, 1983: Large-scale two-dimensional turbulence in the atmosphere. *J. Atmos. Sci.*, **40,** 164–184.

Cehelsky, P., 1987: Multiple equilibria, weather regimes and nonlinear equilibration in a simple baroclinic model. Ph.D. thesis, Massachusetts Institute of Technology, 161 pp.

——, and K. K. Tung, 1987: Theories of multiple equilibria and weather regimes—a critical reexamination. Part II: Baroclinic two-layer models. *J. Atmos. Sci.*, **44,** 3282–3303.

Chen, T. C., and A. Wiin-Nielsen, 1978: Nonlinear cascades of atmospheric energy and enstrophy in a two-dimensional spectral index. *Tellus,* **30,** 313–322.

Gall, R., R. Blakeslee and R. C. J. Somerville, 1979: Baroclinic instability and the selection of the zonal scale of the transient eddies of middle latitudes. *J. Atmos. Sci.*, **36,** 767–784.

Green, J. S. A., 1960: A problem in baroclinic stability. *Quart. J. Roy. Meteor. Soc.*, **86,** 237–251.

——, 1970: Transfer properties of the large-scale eddies and the general circulation of the atmosphere. *Quart. J. Roy. Meteor. Soc.*, **96,** 157–185.

Haidvogel, D. B., and I. M. Held, 1980: Homogeneous quasi-geostrophic turbulence driven by a uniform temperature gradient. *J. Atmos. Sci.*, **37,** 2644–2660.

Hart, J. E., 1981: Wavenumber selection in nonlinear baroclinic instability. *J. Atmos. Sci.*, **38,** 400–408.

Held, I. M., 1978: The vertical scale of an unstable wave and its importance for eddy heat flux parameterizations. *J. Atmos. Sci.*, **35,** 572–576.

James, I. N., 1987: Suppression of baroclinic instability in horizontally sheared flows. *J. Atmos. Sci.*, **44,** 3710–3720.

Klein, P., and J. Pedlosky, 1986: A numerical study of baroclinic instability at large supercriticality. *J. Atmos. Sci.*, **43,** 1243–1262.

Lindzen, R. S., and B. Farrel, 1980: The role of polar regions in global climate and a new parameterization of global heat transport. *J. Atmos. Sci.*, **108,** 2064–2079.

Lorenz, E. N., 1960: Energy and numerical weather prediction. *Tellus,* **12,** 364–373.

——, 1963: The mechanics of vacillation. *J. Atmos. Sci.*, **20,** 448–464.

Moura, A. D., and P. H. Stone, 1976: The effects of spherical geometry on baroclinic instability. *J. Atmos. Sci.*, **33,** 602–616.

O'Brien, E., and L. E. Branscome, 1988: Modes of variability in a low-order two-level model. *Tellus,* **40A,** 358–374.

Panetta, R. L., and I. M. Held, 1988: Baroclinic eddy fluxes in a one-

dimensional model of quasi-geostrophic turbulence. *J. Atmos. Sci.*, **45**, 3354–3365.

Pedlosky, J., 1981: The nonlinear dynamics of baroclinic wave ensembles. *J. Fluid Mech.*, **102**, 169–209.

Reinhold, B., 1988: Structural determinism of equilibrated baroclinic waves in a two-layer model and equivalent barotropy. *Tellus*, **40A**, 375–391.

——, 1989: Comments on "Theories of multiple equilibria and weather regimes—a critical reexamination. Part II: Baroclinic two-layer models". *J. Atmos. Sci.*, **46**, 1861–1864.

Rhines, P. B., 1975: Waves and turbulence on a beta-plane. *J. Fluid Mech.*, **69**, 417–443.

Salmon, R., 1980: Baroclinic instability and geostrophic turbulence. *Geophys. Astrophys. Fluid Dyn.*, **15**, 167–211.

Shepherd, T. G., 1987: A spectral view of nonlinear fluxes and stationary-transient interaction. *J. Atmos. Sci.*, **44**, 1166–1177.

Simmons, A. J., and B. J. Hoskins, 1978: The life cycles of some nonlinear baroclinic waves. *J. Atmos. Sci.*, **35**, 414–432.

Stone, P H., 1972: A simplified radiative-dynamical model for the static stability of rotating atmospheres. *J. Atmos. Sci.*, **29**, 405–418.

——, 1978: Baroclinic adjustment. *J. Atmos. Sci.*, **35**, 561–571.

——, and D. A. Miller, 1980: Empirical relations between seasonal changes in meridional temperature gradients and meridional fluxes of heat. *J. Atmos. Sci.*, **37**, 1708–1721.

Vallis, G. K., 1983: On the predictability of quasi-geostrophic flow: The effects of beta and baroclinicity. *J. Atmos. Sci.*, **40**, 10–27.

——, 1988: Numerical studies of eddy transport properties in eddy resolving and parameterized models. *Quart. J. Roy. Meteor. Soc.*, **114**, 183–204.

——, and J. O. Roads, 1984: Large-scale stationary and turbulent flow over topography. *J. Atmos. Sci.*, **41**, 3255–3271.